

Winter 3-11-2022

# Quantification of Reynolds Shear Stress Wave-Phase Dependence in Fixed-Bottom Offshore Wind Turbine via Quadrant Analysis

Cerrina Mouchref  
*Portland State University*

Bianca Viggiano  
*Portland State University*

Raúl Bayoán Cal  
*Portland State University*

Ondrej Ferčák  
*Portland State University*

Follow this and additional works at: <https://pdxscholar.library.pdx.edu/honorsthesis>



Part of the [Other Mechanical Engineering Commons](#)

Let us know how access to this document benefits you.

---

## Recommended Citation

Mouchref, Cerrina; Viggiano, Bianca; Cal, Raúl Bayoán; and Ferčák, Ondrej, "Quantification of Reynolds Shear Stress Wave-Phase Dependence in Fixed-Bottom Offshore Wind Turbine via Quadrant Analysis" (2022). *University Honors Theses*. Paper 1177.  
<https://doi.org/10.15760/honors.1229>

This Thesis is brought to you for free and open access. It has been accepted for inclusion in University Honors Theses by an authorized administrator of PDXScholar. Please contact us if we can make this document more accessible: [pdxscholar@pdx.edu](mailto:pdxscholar@pdx.edu).

Spring 6-12-2022

# Quantification of Reynolds shear stress wave-phase dependence in fixed-bottom offshore wind turbine via quadrant analysis


Cerrina Mouchref

Bianca Viggiano

Raul Bayoan Cal

Ondrej Fercak

Follow this and additional works at: <https://pdxscholar.library.pdx.edu/honorsthesis>

 Part of the [Applied Mechanics Commons](#), and the [Other Mechanical Engineering Commons](#)  
**Let us know how access to this document benefits you.**

---

This Thesis is brought to you for free and open access. It has been accepted for inclusion in University Honors Theses by an authorized administrator of PDXScholar. Please contact us if we can make this document more accessible: [pdxscholar@pdx.edu](mailto:pdxscholar@pdx.edu).

Quantification of Reynolds shear stress wave-phase dependence in fixed-bottom  
offshore wind turbine via quadrant analysis

by

Cerrina Mouchref

An undergraduate honors thesis submitted in partial fulfillment of the

requirements for the degree of

Bachelor of Science

in

University Honors

and

Environmental Engineering

Thesis Adviser

Raúl Bayoán Cal

Portland State University  
2022

# Quantification of Reynolds shear stress wave-phase dependence in fixed-bottom offshore wind turbine via quadrant analysis

Cerrina Mouchref, Ondrej Ferčák, Bianca Viggiano, Raúl Bayoán Cal  
(Dated: March 21, 2022)

## I. ABSTRACT

As the need for a reliable renewable energy supply is increasing, many have looked to offshore wind because they hold more potential for power production than onshore wind. Interests in expanding offshore wind energy has brought along many challenges when it comes to understanding the complex dynamics experienced offshore, including the relationship between the wind-turbine generated wakes and ocean waves. This experimental study characterizes the relationship between Reynolds shear stress and the phase of surface waves above the air-sea interface in the wind-turbine wake region. The experimental setup combines a wave tank, wind tunnel, and a fixed-bottom wind turbine. Particle image velocimetry (PIV) is performed for three successive planes to visualize wave-wake interactions far downstream. Triple decomposition is performed to resolve phase-dependent velocity fields. Quadrant analysis was utilized to provide insights into momentum transport and Reynolds stress composition. Shear stress profiles behind the turbine were observed during three wave conditions: no wave, long wave, and short wave. Ensemble averaged profiles reveal a rotating wake region of reduced momentum behind the turbine that is not dependent on wave features. Phase averaged velocity profiles show Reynolds stress wave-induced phase-averaged fluctuations that follow the curvature of the waves. Significant Reynolds stress dependence on wave phase is observed primarily in quadrants I and III and altered the position of the turbulence events. The results indicate a correlation between surface waves and turbulent wind-wake interactions that can be utilized for design optimization and control strategies.

## II. INTRODUCTION

With an increase in global energy consumption, there has been a push to find a sustainable energy supply. For many years, wind energy has provided a reliable option to fulfill the increasing energy demands. [1]. Complex interactions between ocean waves and Reynolds stress that affect the loading and energy production of the turbines have yet to be fully understood. Categorizing and understanding variations in Reynolds stresses influenced by wave motion can contribute to the maximization of energy production through design and spacing of turbines [2].

As more wind turbines are being placed offshore, additional considerations with respect to fatigue loading must be made due to drastically different environmental conditions than those that exist for onshore turbines. One must take into account environmental loading from waves, currents, and tides [3]. Offshore wind is highly dependent on dynamic interactions between ocean waves and the atmospheric boundary layer (ABL). Locally generated short waves can be regarded as moving surface elements that affect the ABL through surface friction. Interaction between ocean waves and the ABL transfers momentum and energy into the mean airflow which influences turbulent flow and the vertical wind speed profile, and induces oscillatory motion [4]. Wave dependence can be detrimental to the life cycle of the turbine [5]. Wake dynamics behind a single turbine have a significant influence on performance and reliability [6]. Shear stress profiles in the near-field can provide insights used for control strategies to maximize power extraction. Far-field shear stress profiles are used to address the effect of the wake on downstream turbines and the environment [7]. An offshore wake from a small wind farm has been seen to propagate for 14 km over the water [8]. Offshore wind farm wake dynamics propagate farther than onshore wind due to less atmospheric turbulence. Inter-farm effects of offshore wind turbines is becoming a significant issue as offshore wind capacity has been growing. [7]. Understanding the dependence of waves on Reynolds shear stress profiles has the potential to make designing wind turbines for fatigue loading more effective and therefore contributing to a longer turbine lifetime and lower overall cost for offshore wind.

Loss of momentum within the wind turbine wake will negatively impact power extraction in downstream turbines. Large wind turbine farms consist of tens or hundreds of wind turbines arranged in large arrays, which leads to the concern about downstream turbine efficiency. Wind farms experience a phenomenon where the wake created by the upstream turbine will experience a velocity deficit and turbulence turns intense as it moves downstream. The loss of momentum within the wind turbine wake will negatively impact power extraction in downstream turbines and increase fatigue loading [9]. Power extraction decreases as currents move further downstream and significantly reduces the overall power output of the wind farm [5]. Wake interference among wind turbines in large arrays may suffer up to 30 percent power loss and up to 80 percent more fatigue loads [10]. In a study conducted by Meneveau et al., downwind swells were found to have a considerable effect on power extraction and power output in offshore wind turbines [11].

Wind speed in the lower portion of the boundary layer oscillates with fast wind above the swell trough and slow wind above the swell crest resulting in oscillatory wind speed due to wave propagation. An upward flux of kinetic energy due to wind accelerating above the swell increases extracted wind power in turbines at wind speeds of 7m/s and 10 m/s [12].

One technique which provides insight into momentum transport and Reynolds stress composition, is quadrant analysis. This method can be employed on the turbulent boundary layer to explore dominant contributions to the Reynolds shear stress by separating the flow into four events based on velocity fluctuations. Quadrant analysis has been used to compare Reynolds stress profiles in turbulent boundary layers over rough walls [13], analyze air-sea interactions over wind generated surface waves [14], characterization of the wake behind a cylinder [15, 16], and the characterization of flow over plant canopies. Yue et al. [11] and [17] utilized quadrant analysis to analyze results of a large eddy simulation over a mature cornfield. Both studies found that sweeps and ejections played a dominant role in turbulent kinetic energy evolution inside the canopy. Results from a study of turbulent airflow over wind generated surface waves show an intense wave-phase dependent modulation by the wave field on the turbulence in the airflow. Results observed a dominance of Q1-Q3 events upwind of crests, an equivalence of all quadrants above crests, a clear dominance of Q2-Q4 downwind of crests, and a very slight dominance of Q2-Q4 events over troughs [14]. Viestenz and Cal used quadrant analysis to characterize turbulent velocity statistics of the wake flow. Results found that sweeps and ejections are dominant above the hub height while inward and outward interactions are more influential below the hub height. Results also found sweeps tend to decrease above the top tip contrasted by an increase of ejections above the top tip [18]. Dominant events in a wind turbine array were found to be sweeps and ejections [12]. In a study conducted on a 3x3 wind turbine array model, kinetic energy and vertical momentum transport are correlated with the Reynolds shear stresses, thus highlighting the importance of vertical transport in wake recovery. [19]. Wake characteristics effect fatigue loading, power extraction, and efficiency maximization strategies. Currently, not much is known about the characteristics of the external flow structures that influence kinetic energy entertainment[2]. Characterizing Reynolds shear stress can provide insight on flow structures that influence wake recovery.

Particle image velocimetry (PIV) can be utilized to generate 2D velocity fields for quadrant analysis, and has been extended to scaled wind farm arrays [20]. PIV has been used to study different flow characteristics in a turbine array such as dynamic stalls in a vertical axis wind turbine [21] and the wake behind a turbine [22, 23]. In an experimental study by Buckley and Veron [24] PIV was combined with laser induced fluorescence (LIF) techniques to track airflow dynamics above the air-sea interface. The study found that the turbulent boundary layer was dominated by ejections and sweeps and the production of turbulent kinetic energy was influenced by wave phase.

An additional design challenge for wind turbine farms is the dynamic coupling of the ocean-wind and waves. To overcome challenges of the shifting phase of the ocean wave at the air-sea interface, introducing a temporal component, the air-sea interface has been modeled as a complex rough surface. Yang, Meneveau, and Shen created a dynamic model by classifying waves as moving roughness elements within a rough surface in order to model the turbulent boundary layer. They found that "waves have an appreciable effect on the wind farm performance"[25]. In order to further characterize wave phase dependence, Xiao and Yang [26], performed triple decomposition to decompose turbulent fluctuations and the phase averaged mean to define an instantaneous phase-averaged dependent fluctuation term [5]. Understanding the dynamic coupling between ocean waves and Reynolds shear stress can provide a better insight offshore wind site conditions.

In this study, the wake effects due to a turbine and the wind-wave interactions are studied to better characterize the flow field events behind a fixed-bottom offshore wind turbine. Particle image velocimetry as well as laser induced fluorescence were implemented to analyze the modulations of the turbine wake based on deep-water ocean waves. Analytical descriptions are presented in section III, followed by details of the experimental setup and data processing techniques in section IV. Section V provides the first and second-order statistics of the flow field as well as conditional averages based on quadrant analysis. Concluding remarks are included in section VI.

### III. THEORY

The exchanges in momentum within the boundary layer when a wind farm is present can be understood through the Navier-Stokes equation as it takes into account the force imposed by the turbines within the flow acting as momentum extracting elements. Based on this, the Reynolds-averaged Navier-Stokes equation for steady, incompressible, and inviscid flows is written in the streamwise direction as,

$$\bar{u} \frac{\partial \bar{u}}{\partial x} + \bar{v} \frac{\partial \bar{u}}{\partial y} = -\frac{1}{\rho} \frac{d\bar{p}}{dx} - \frac{\partial}{\partial x} \overline{u'u'} - \frac{\partial}{\partial y} \overline{u'v'} - \bar{f}_x, \quad (1)$$

where  $u$ , and  $v$ , and  $w$  are the instantaneous streamwise and vertical transverse velocities respectively in the  $x$  and  $y$  directions. Once the Reynolds decomposition and averaging has been performed, primes indicate turbulent fluctuations and overbars indicate time-averaging. The left side of the equation represents advection terms. The  $\overline{u'v'}$  is the Reynolds shear stress and accounts for vertical recovery of momentum in the wake [12].  $\rho$  represents the fluid density.  $\overline{f_x}$  represents the thrust effect of the wind turbine which acts only in the region where wind turbines are located. Viscous terms are neglected due to farness from solid boundaries.

Given the dynamics of the lower boundary, now containing a free surface, wave-phase dependence of Reynolds stresses become of interest. Phase-averaging techniques are used to decompose the velocity field as is presented in Buckley and Veron [24]. Thus, instantaneous velocity profiles can be averaged according to their phase. First, individual instantaneous velocity fields,  $u_\phi(x, y)$ , can be decomposed using a standard Reynolds decomposition to the sum of the mean,  $\bar{u}_\phi(x, y; \phi)$  and the turbulent deviations,

$$u_\phi(x, y) = \bar{u}_\phi(x, y; \phi) + u'_\phi(x, y). \quad (2)$$

A dependence on  $\phi$  is introduced as the wave phase, while  $x$  and  $y$  are the streamwise and wall-normal locations, respectively. The phase averaged mean velocity,  $\bar{u}_\phi(x, y; \phi)$ , can be further decomposed into the ensemble mean (or average of all phases),  $\bar{u}(x, y)$  and phase averaged deviations  $\tilde{u}(x, y, \phi)$  yielding the following relationship:

$$\bar{u}_\phi(x, y; \phi) = \bar{u}(x, y) + \tilde{u}(x, y, \phi). \quad (3)$$

The phase-averaged mean is not resolved from the ensemble mean, it is a composition of the ensemble mean and the phase-averaged deviation. Substitution of Eq. (3) into Eq. (2), results in triple decomposition:

$$u_\phi(x, y) = \bar{u}(x, y) + \tilde{u}(x, y, \phi) + u'_\phi(x, y), \quad (4)$$

providing clear indication that these quantities are related. Therefore additional conditioning of the velocity signals is required to quantify influence of the wave-wind interface on the wake dynamics the influence of the wave-wind interface.

Analysis of dominant contributions to the Reynolds shear stress can be characterized through a conditional sampling technique called quadrant analysis.[12]. Velocity fluctuations are characterized into four types of events based on the respective signs of streamwise and wall-normal fluctuating velocity components designated as followed: Q1, outward interaction ( $u'_\phi, v'_\phi > 0$ ); Q2, ejection ( $u'_\phi < 0, v'_\phi > 0$ ); Q3, inward interaction ( $u'_\phi, v'_\phi < 0$ ); and Q4, sweep ( $u'_\phi > 0, v'_\phi < 0$ ). These four events can be represented visually by creating a plane axis with  $u'_\phi$  on the abscissa and  $v'_\phi$  as the ordinate see figure 1[18]. The average stresses of each of the four events is decomposed using the phase averaged deviations  $u'_\phi(x, y)$ . The average shear stress for each quadrant is defined as

$$\langle u'_\phi v'_\phi \rangle = \frac{1}{N} \sum_{m=1}^N I_k(u'_\phi, v'_\phi) u'_\phi v'_\phi \quad (5)$$

$N$  is ensemble of samples in quadrant  $k$ , where  $k= 1, 2, 3, 4$ . The function  $I_k(u'_\phi, v'_\phi)$  is defined as

$$I_k(u'_\phi, v'_\phi) = \begin{cases} 1, & \text{If } (u'_\phi, v'_\phi) \text{ is in quadrant } k \\ 0, & \text{otherwise} \end{cases} \quad (6)$$

Quadrant events can be physically interpreted as revealing the directionality of the flow in comparison with the mean flow. For example, ejections represent turbulent bursts upwards at velocities slower than the mean, while sweeps represent turbulent burst downward in the positive streamwise direction [12]. Events in quadrants 2 and 4 cause a downward convection of streamwise momentum while quadrants 1 and 3 provide an upward flux [18].

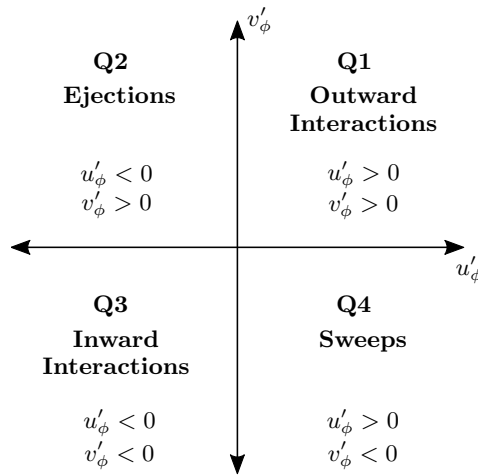


FIG. 1. Definition of the four quadrant for the wake of the wind turbine based on the phase-dependent fluctuating velocities  $u'$  and  $v'$ .

#### IV. EXPERIMENTAL METHODS

Experiments were performed at Portland State University in the closed loop wind tunnel in which the floor was replaced by a 0.3 m deep water tank to replicate conditions impacted by deep open waves. The tank spanned the entire experimental test section of the tunnel which is 0.8 m by 1.2 m in cross-section and 5 m in length. A scaled wind turbine was placed on a stiff support within the water tank, situated just below the surface of the water, see figure 2. The turbine has a diameter,  $D$ , of 0.15 m, resulting in a geometric scaling ratio to a full size wind turbine of 1:600, based on a rotor design following the work of [27]. A tip speed ratio of 5 was chosen for the experiments with a  $c_p \approx 0.25$  at this rating.

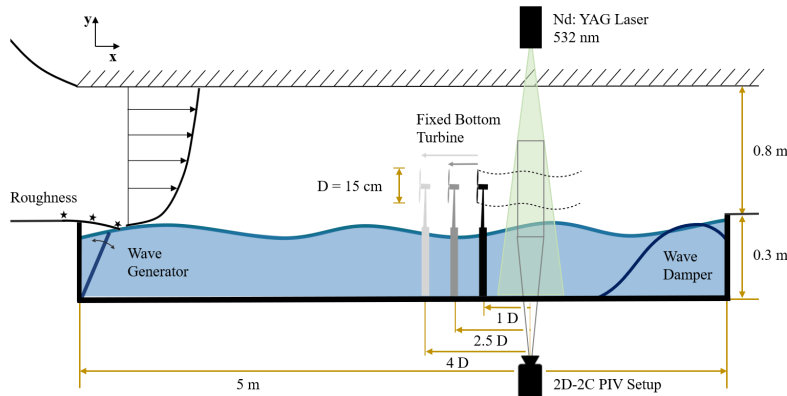


FIG. 2. Experimental setup of the wind tunnel (not to scale).

At the entrance of the tunnel test section a wave paddle produces scaled deep-water waves, see figure 3(a) and 3(b). The wave and wind interface was measured using LIF visualization and the wave height and frequency was extracted for each snapshot. Finally, a damper was placed at the end of the tunnel to absorb incoming waves. Three conditions were used to quantify the impact of wave frequency on wake effects of the turbine. Two active conditions and one passive (no wave paddle) condition, with parameters of the two active cases presented in table I. The inflow wind tunnel speed varied from  $2.5 \text{ ms}^{-1}$  to  $5.5 \text{ ms}^{-1}$ . The turbulence intensity for these conditions was 6-7% at the turbine hub height for the 1.25 Hz (long) waves and  $\sim 8\%$  for the 2.0 Hz (short) wave inputs. A zero-pressure gradient boundary layer was ensured by a diverging tunnel ceiling. Extensive details on the cameras, sensors and post processing are found in [5].

Wave condition	Frequency [Hz]	Period [s]	Amplitude [m]	Speed [m/s]	wavelength [m]
Short	2.00	0.5 ( $\pm 0.01$ )	0.020	0.7 ( $\pm 0.03$ )	0.36 ( $\pm 0.02$ )
Long	1.25	0.8 ( $\pm 0.01$ )	0.013	1.2 ( $\pm 0.08$ )	1.00 ( $\pm 0.06$ )

TABLE I. Wave tank experimental parameters.

Particle image velocimetry was employed to create the velocity fields. Three PIV planes of data were extracted at  $1D$ ,  $2.5D$  and  $4D$  with the measurement window parallel to the streamwise velocity, as shown in figure 2. Images were captured with a 4 megapixel CCD camera using a Nd:YAG double pulsed laser. A seeding generator aerosolized diethyl-hexyl sebacate into the the tunnel with constant density during the measurements. 3000 individual snapshots were taken at 4Hz for each of the PIV planes and inflow conditions. The data were processed in Davis 8.4 using a cross-correlation algorithm with one pass with an interrogation area of  $64 \times 64$  pixels and 50% overlap followed by a pass with an interrogation size of  $32 \times 32$  pixels.

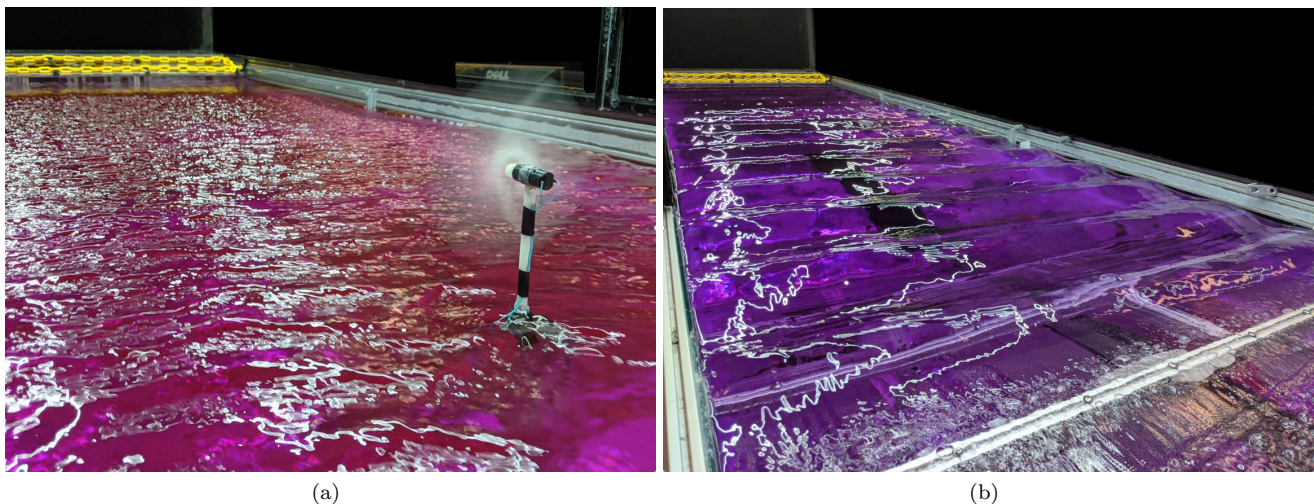


FIG. 3. Generation of the waves within the wind tunnel for a) 2 Hz waves and b) 1.25 Hz waves.

## V. RESULTS

The Reynolds shear stress is investigated in order to reveal possible dependence on wave phase in the wake of a fixed-bottom wind. In the shear stress profiles and quadrant analysis figures that follow, the solid black line marks the location of the rotor hub, the component of the turbine that holds the blades and connects them to the main shaft, on the vertical axis. The dashed lines represent the location of the top and bottom tip of turbine blades.

The ensemble averaged normalized streamwise velocity  $\bar{u}/u_\infty$ , wall-normal velocity  $\bar{v}/u_\infty$ , and Reynolds stress  $\overline{u'v'}/(u_\infty)^2$  at a wind tunnel speed ( $v_L$ ) of 2.5 m/s and wave frequency ( $\omega_{1.25}$ ) of 1.25 Hz is shown in Figure 4. The  $x$  and  $y$  locations are normalized by the diameter ( $D$ ) of the rotor. Inflow is from left to right and the turbine rotor is located at  $x/D = 0$ . Extraction of energy from wind across a turbine rotor produces a wake region downstream with reduced velocity and increased turbulence. The streamwise velocity profile shows a canonical wake profile with a region of reduced momentum directly behind the turbine rotor, which recovers slowly as it moves downstream. Increased velocity, reaching nearly that of the free stream is reached quickly above the top tip of the turbine. A slight increase in  $\bar{u}$  is also observed below the bottom tip. Wall-normal velocity,  $\bar{v}/u_\infty$ , presents much smaller magnitudes due to bulk flow in the streamwise direction. Negative wall-normal velocity is observed behind the turbine rotor where the fluid is being entrained from above the top tip during wake recovery. Upward (positive) wall-normal velocity is equally observed as fluid is entrained from below the bottom tip. Time-averaged streamwise and wall-normal velocity are discussed in great detail in Ferčák et al. [5].

For the normalized turbulent shear stress,  $\overline{u'v'}/u_\infty^2$ , shown in Figure 4, there is a region at the wake center where the shear stress is zero with positive stresses below and negative stresses above. This indicates wake rotation caused by



rotational blade induced helical tip vortices [28], depicted by large streaks of stresses that show acute features located at the dashed lines. Increased turbulence caused by wake rotation results in less power being available for subsequent turbines [6]. As the wake recovers farther downstream, regions of positive and negative shear stress dissipate and occupy a larger vertical range. A decrease in wind speed across the rotor area corresponds to a greater downstream area [29], causing the low pressure wake region to expand as it moves downstream until it eventually dissipates as equilibrium is reached with the surrounding airflow [30, 31].

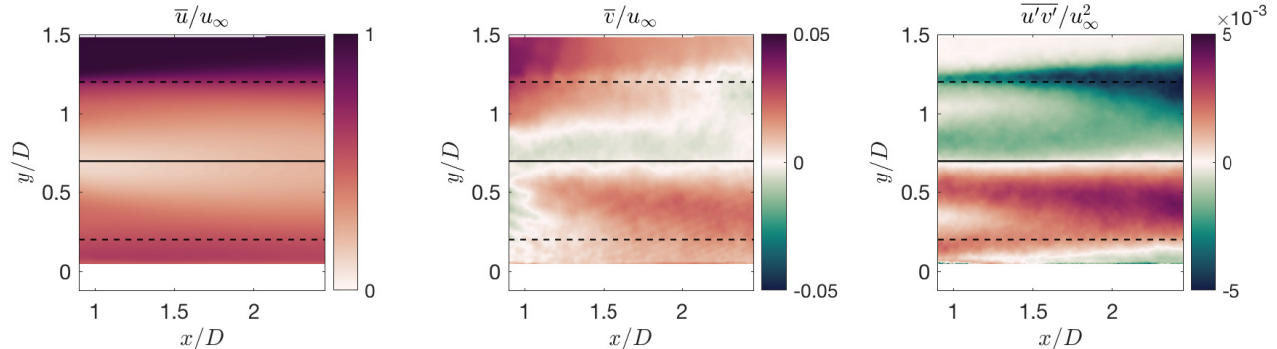


FIG. 4. Time averaged streamwise, wall-normal and Reynolds shear stress for the  $v_L \omega_{1.25}$ .

For comparison between boundary conditions of the experiments, the Reynolds stress for all cases is presented as profiles in averaged in space over the streamwise locations for  $1 < x/D < 2.5$  and over all time steps. The Reynolds stress profiles for each of the six ensemble-averaged inflow conditions prior phase averaging are shown in Figure 5. All of the inflow conditions induce consistent profiles and closely resemble the no-wave boundary condition ( $v_L \omega_0$ ). The disruption of airflow induces wake rotation behind the turbine, producing a negative shear stress above the rotor and a positive shear stress below the rotor. The stress profile is highly undulated in the near field then as turbulence turns intense moving downstream, the wake begins to recover and shear stress magnitude increases into an expanding area as these undulations disappear. The ensemble averaged profiles representing the six different inflow conditions follow the same pattern and produce nearly identical shapes when wave phase is not considered. Positive shear stress in the lower portion of the turbine suggests using control strategies[5]. The persistence of the Reynolds shear stress in the far-field indicates downstream turbines could be affected by structural loads as well as providing insights on optimal turbine placement [32].

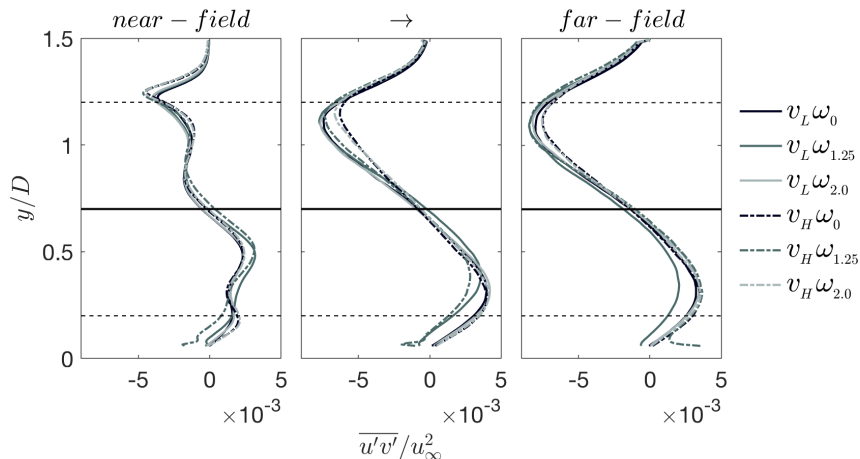


FIG. 5. Profiles of the Reynolds stress,  $\overline{u'v'}/u_\infty^2$  for all cases as a function of wall-normal location. The profiles are averaged in time and in space from  $1 < x/D < 2.5$ .

Figure 6 shows the four wave-phase ( $\phi$ ) averaged Reynolds stress profiles ( $u'_{\phi_i} v'_{\phi_i}$ ) at quarter wave increments for the long wave condition ( $\omega_{1.25}$ ) and low wind tunnel speed ( $v_L$ ) of 2.5 m/s. The motion of the wave at each phase is determined by the relative position of the crest and the trough of the wave depicted by the cropped white region

at the bottom of the image. Similar to the Reynolds stress profile seen in Figure 4, there is a region where the shear stress is zero at the wake center, behind the wind turbine hub that marks a switch from positive to negative shear stress. The wake center deviates in the shear profiles and follows the concavity of the wave shape, indicating a phase dependence. The positive and negative shear stress regions above and below the wake center also experience a phase dependence and align with the wave phase profile. Acute areas of positive shear is observed at the leading edge of the wave followed by a negative shear on the trailing edge of the wave. There are extended tails of negative shearing events that follow the wave, wherein the flow is being entrained and advancing the flow. The coherent structures in the shear stress profile have a high correlation to power production of consecutive turbines, which can be exploited through control strategies and turbine spacing [33].

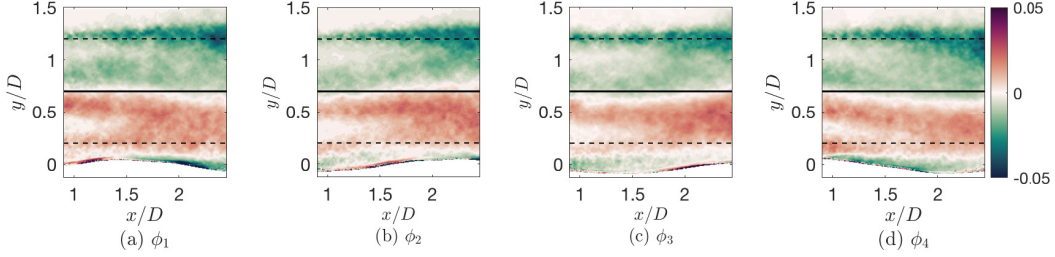


FIG. 6.  $\overline{u'_{\phi_i} v'_{\phi_i}}$  for the four phases ( $\phi_1 - \phi_4$ ) for the case  $v_L \omega_{1.25}$  for the near-field location.

To quantify the effects of the stress features, the flow field is conditioned further to isolate and characterize these trends. Figure 7 utilizes quadrant analysis to depict the ensemble Reynolds stress ( $u'v'$ ) and phase averaged stress for  $\phi_1$ , for the long wave condition ( $\omega_{1.25}$ ) and low wind tunnel speed of 2.5 m/s in the near-field. Recall that quadrant events can be physically interpreted as revealing the directionality of the flow in comparison with the mean flow [18], i.e., advancing or impeding the flow, entraining or ejecting. Quadrants 2 and 4 have peak magnitudes slightly larger than quadrants 1 and 3. A dominance of ejections and sweeps (quadrants 2 and 4) are observed behind top tip of the turbine blade and the nacelle, which contributes to the negative Reynolds stress in those regions. This is consistent with the general trend that sweep and ejection events are prominent in high shear regions of boundary layer flows since streamwise and wall-normal velocity fluctuations are typically anti-correlated i.e.  $-\overline{uv}$  [34]. Again, the dissipation of the structure as it progresses downstream is observed in Q2 and Q4 as was observed in the total stress contributions in figure 4. Events in quadrants 1 and 3 are localized between the bottom tip of the turbine blade and near the wave. This is consistent with results reached by Viestenz and Cal, where sweeps and ejections are dominant above the hub height while inward and outward interactions are more influential below the hub height [18]. On-shore turbine wake flow presents large structures at the top tip in Q2 and Q4 [12], as is observed for the fixed bottom turbine cases presented in figure 7 as well. In addition, structures are observed at the bottom of the interrogation area and cause inward and outward interactions which are less commonly observed in on-shore turbine wakes. This addition is likely due to wave-wind interactions causing correlation of the streamwise and spanwise fluctuations. When comparing the total stress field, figure 7(a), to the phase averaged stress field, figure 7(b), there is a clear phase dependence seen in all four quadrants. In quadrants 1 and 3, phase dependence can be seen as shear stress fields are curved following the shape of the wave. Wave phase dependence is still seen in quadrants 2 and 4 with a slight curve in the shear stress field of lesser magnitude than quadrants 1 and 3.

To interpret the effects of the phase on the conditioned flow, quadrant analysis is applied and profiles are compared. Figures 8 and 9 depict quadrant analysis of the Reynolds shear stress profiles ( $u'_{\phi_i}, v'_{\phi_i}$ ) at a low wind tunnel speed ( $v_L$ ) of 2.5 m/s at long ( $\omega_{1.25}$ , figure 8) and short ( $\omega_{2.00}$ , figure 9) wave conditions for all four phases. The profiles are obtained by time averaging then spatial averaging over the respective streamwise locations to investigate near to far-wake dynamics. Reynolds shear stress in all four quadrants and all conditions dissipates moving downstream as undulations disappear and magnitude increases. Peak magnitudes in quadrants 2 and 4 are larger than quadrants 1 and 3. Negative peak magnitudes occur in quadrants 2 and 4 between the rotor and the top tip of the turbine blade. Positive peak magnitudes occur in quadrants 1 and 3 between the the water surface and the bottom tip of the blade. A phase dependence can be seen in all four quadrants as the stress profiles are shifted vertically relative to the stress profile of the condition with no-wave ( $v_L \omega_0$ ). For the long wave condition depicted in figure 8, large deviations from the no-wave condition are seen in quadrants 1 and 3 due correlation with wave phase. Deviations due to wave phase seen in quadrants 2 and 4, located much farther from the air water interface, are much smaller than quadrants 1 and 3. Larger phase deviations are seen in quadrant 2 and 4 for the short wave condition than the long wave conditions. In addition, quadrants 1 and 3 have less phase dependence for the short wave than the long wave.

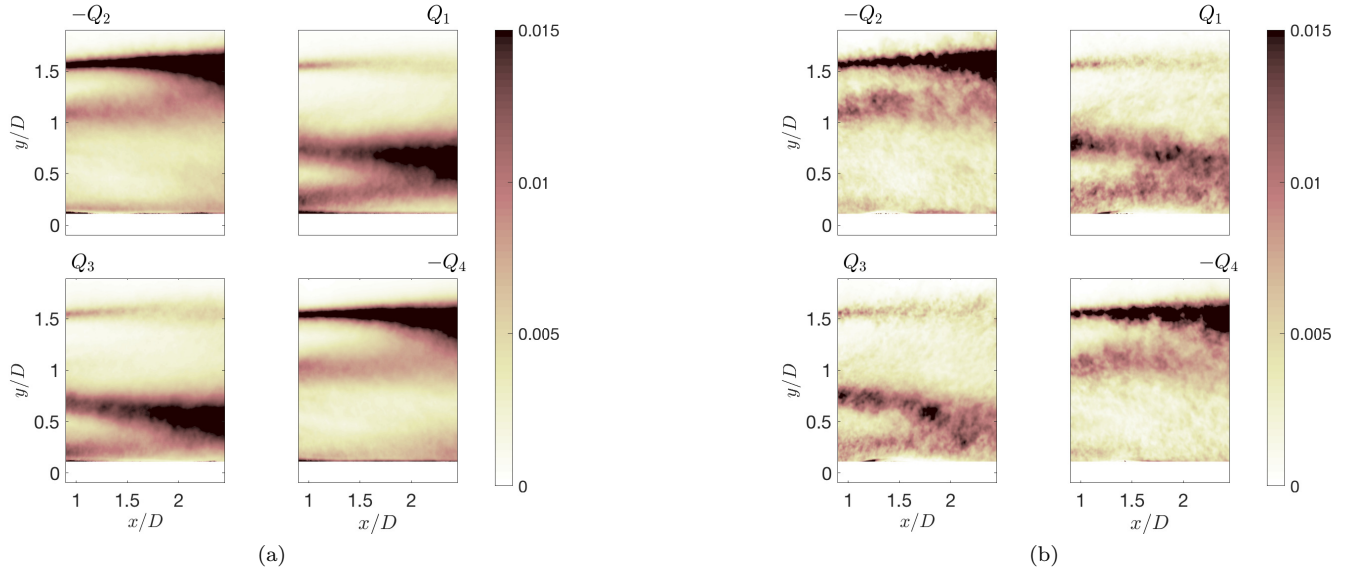


FIG. 7. Quadrant contours of the near field of the case  $v_L \omega_{1.25}$  for (a) the total stress  $u', v'$  and (b) the phase-averaged stress  $u'_{\phi_1}, v'_{\phi_1}$ .

The dependence on the wave for increased stresses near the wave-wind interface could cause increased vibrations and fatigue to the turbines and the mast when operating in off-shore, fixed bottom conditions. This is most noticeable by the large stresses observed in the far-field for Q1 and Q3 in figures 8 and 9, which occur just above the bottom tip of the rotor. Q1 and Q3 turbulent events can influence power production of consecutive turbines. Understanding how phase influences Reynolds shear stress can provide insights on wake recovery which can be used to maximize power extraction in downstream turbines through wake deviation control strategies and turbine spacing.

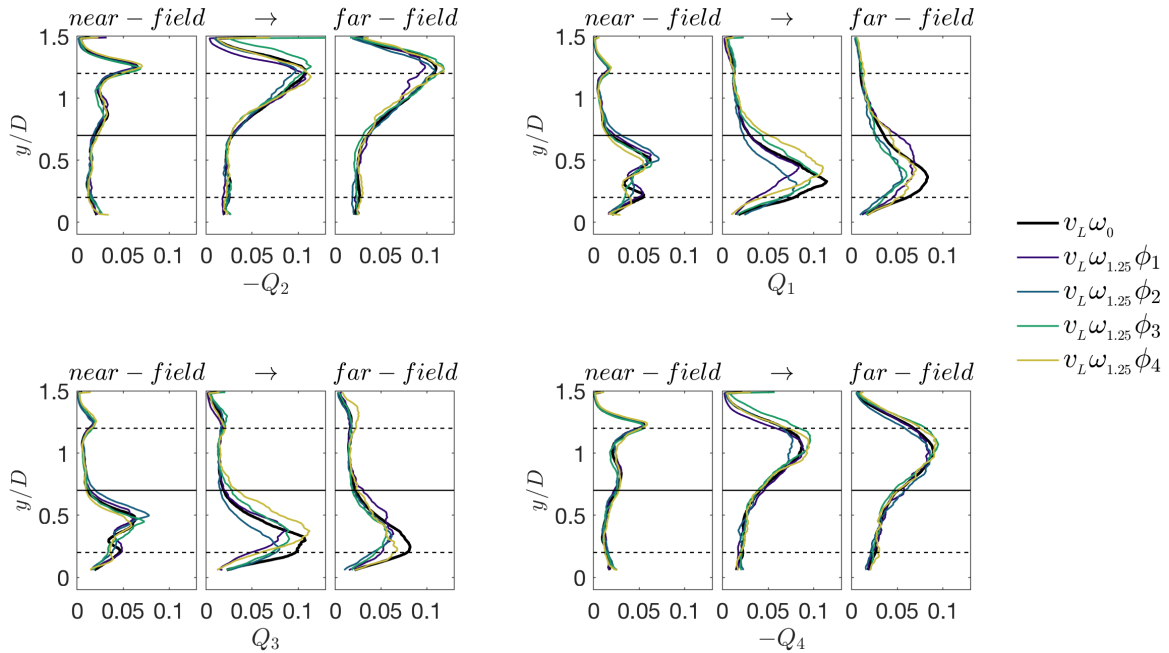


FIG. 8. Comparison of the profiles of the quadrant analysis, for all phases of  $v_L \omega_{1.25}$ . The case with no wave paddle input is included for comparison as well. The profiles are summed over their respective streamwise sublocations in near-field to far-field and all curves are normalized by the total snapshots of each phase averaged subset of data.

Figure 10 depicts the difference between the Reynolds stress profiles of Q2 (ejections) and Q4 (sweeps). Ejections

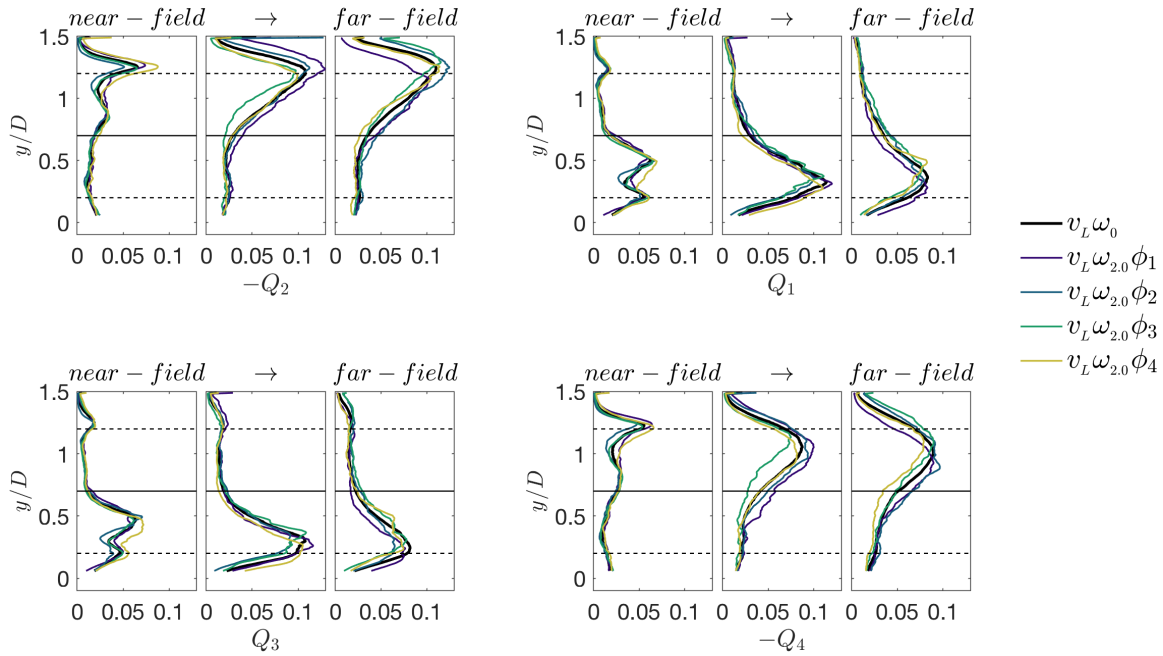


FIG. 9. Comparison of the profiles of the quadrant analysis, for all phases of  $v_L \omega_{2.0}$ . The case with no wave paddle input is included for comparison as well. The profiles are summed over their respective streamwise sublocations in near-field to far-field and all curves are normalized by the total snapshots of each phase averaged subset of data.

and sweeps dominate the flow at different spots. When the difference is negative, ejections dominate the flow, and when the difference is positive sweeps dominate the flow. Recall that ejections(Q2) represent turbulent bursts upwards at a streamwise velocity slower than the means and sweeps(Q4) represent turbulent bursts downwards in the positive streamwise direction. The difference in magnitude between the rotor center and the top tip due to the fact that sweeps increase in that range. The contribution of sweeps at this height is due to the passage of the rotor as these events tend to be caused by the rotor acting as an obstruction and forcing the flow downwards [18]. Above the top tip, sweeps decrease and ejections increase making the difference magnitude negative in this region. These results are consistent with previous studies that found that sweeps decrease above the top tip contrasted by an increase in ejections above the top tip [18]. A slight phase dependence is seen in the difference between Q2 and Q4 as the stress profiles are offset from the no wave condition. Differences in sweeps and ejections are correlated to gradients of second-order correlation terms, and can therefore be utilized in second-order closure models [35].

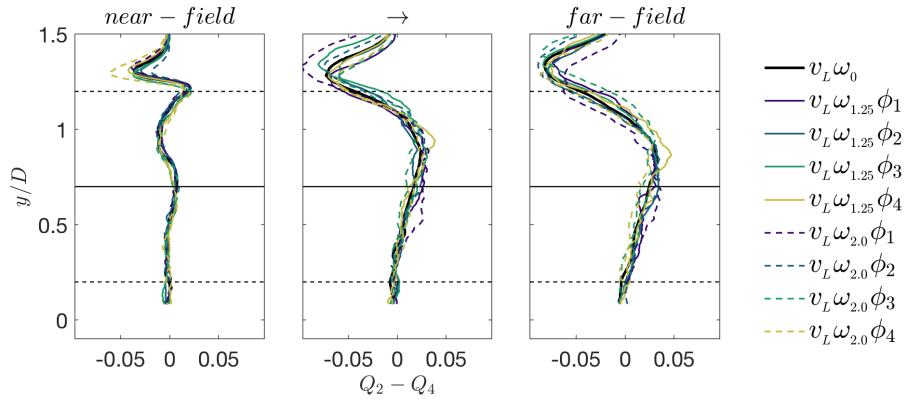


FIG. 10. Quantification of the ejections and sweeps associated with the low speed cases.

Figure 11 contains the difference between the Reynolds stress profiles of Q1 (outward interactions) and Q3 (inward interactions). When the values of the profile are positive, outward interactions dominate the flow and when the profile

is negative, inward interactions dominate the flow. Outward interactions represent turbulent bursts upwards in the positive streamwise direction while inward interactions represent turbulent bursts downwards at a velocity slower than the mean. The strong correlation between these events and wave phase is seen as the phase averaged stress profiles deviate greatly from the no-wave condition. A dominance in inward interactions develops and magnitude peaks above the top tip and below the bottom tip of the turbine. The difference profile switches signs and becomes positive as outward interactions dominate the flow between the bottom tip and the top tip with a magnitude that peaks close to the rotor height. Phase dependence alters the location of quadrant events 1 and 3 as well as 2 and 4 relative to one another observed in Figure 11 and Figure 10. Quantifying the difference magnitude between Q2 and Q4 events as well as Q1 and Q3 events provides insight on the flow mechanisms that influence wake recovery throughout the wake region.

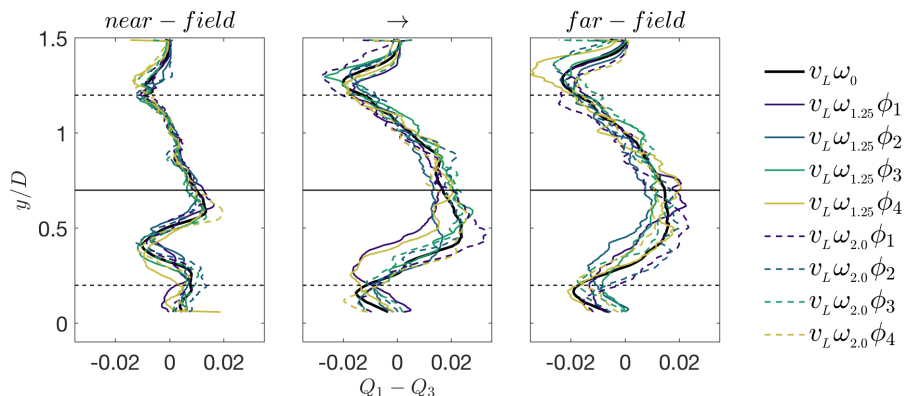


FIG. 11. Differences of the inward and outward interactions based on the quadrant analysis for all low speed cases considered.

## VI. CONCLUSIONS

This study focused on scaled fixed-bottom turbines at two different wind speeds and three wave conditions in a closed loop wind tunnel in which the floor was replaced by a water tank. PIV measurements were collected at three downstream locations to generate velocity fields and detect instantaneous wave profiles for phase averaging. Phase-averaged shear stress profiles were divided into four quadrants based on the respective signs of the streamwise and vertical velocity components to further characterize to dominant contributions to Reynolds shear stress. Results found that wave phase influences the vertical location of the wake center and stress fields. The wake center and stress field were shifted vertically based on the concavity of the wave. Significant wave-phase dependence can help build a better understanding of complex dynamics experience by offshore wind turbines. The results illustrate a more complete picture of offshore wind-energy dynamics which have useful implications for design optimization and control strategies [5].

Further characterizing the Reynolds shear stress into four quadrants shows that in addition to sweeps and ejections between the hub and the top tip, there is an increase in inward and outward near the air-water interface. Large sweep and ejection structures are often seen in high-shear boundary layer flows as well as wake regions behind onshore wind turbines [11, 12, 17]. Inward and outward interactions are less prevalent in boundary layer flows since streamwise and wall-normal velocity are typically anti-correlated[34]. The increase inward and outward interactions is likely caused by wind-wave interactions causing a correlation between  $u'$  and  $v'$ . Increased stress events behind the turbine can influence fatigue loading and power production of downstream turbines. A better understanding of Reynolds stress dependence on wave phase can lead to improved wake recovery models as well as influence the use of control strategies and turbine spacing.

Profiles depicting quadrant analysis for all four phases shows a wave phase dependence is all four quadrant events as stress profiles are shifted in the vertical direction and locations of peak magnitudes vary from the no wave condition( $v_L \omega_0$ ). Differences in the magnitude of phase dependence when comparing the long wave and short wave boundary conditions were seen. For the long wave inflow condition, large deviations from the the no wave condition can be seen in quadrants 1 and 3 in addition to smaller deviations seen in quadrants 2 and 4. However for the short wave condition, Larger phase deviations are seen in quadrant 2 and 4 than quadrants 1 and 3. Quantification of differences in ejections and sweeps(Q2-Q4) showed that sweeps increased in the between the rotor and top tip, and

above the top tip sweeps increase and ejections increase. Differences in Q2 and Q4 events can be used to assess the effectiveness of second-order closure models[18]. The difference magnitude between quadrants 1 and 3 deviate greatly from the no wave condition due to a strong phase dependence near the air-water interface where these stress events occur. Inward interactions(Q3) dominate the flow above the top tip and below the bottom tip of the turbine blades. Outward interactions dominate the flow between the bottom tip and top tip with a maxima close to the rotor hub.

Reynolds shear stress undulations need to be considered for optimization, siting, modeling, and maximizing power production [5]. Waves induce a change in momentum direction observed through increased quadrant 1 and 3 events. Further experiments should be conducted to build off the findings of this study. This analysis focused on dynamics behind one turbine. A study should look at the dynamics of an array of turbines to see how the phenomena discussed in this study applies to power production in turbine farms. Studies should be extended to include results utilizing control strategies, floating wind turbines, spacing techniques, etc. Further studies are pertinent in order to fully characterize complex dynamics experienced by offshore wind turbines.

- 
- [1] D. Yang, C. Meneveau, and L. Shen, Effect of downwind swells on offshore wind energy harvesting—a large-eddy simulation study, *Renewable Energy* **70**, 11 (2014).
  - [2] H. F. Kadum, D. Knowles, and R. B. Cal, Quantification of preferential contribution of reynolds shear stresses and flux of mean kinetic energy via conditional sampling in a wind turbine array, *Journal of Fluids Engineering* **141** (2019).
  - [3] J.-T. Horn and B. J. Leira, Fatigue reliability assessment of offshore wind turbines with stochastic availability, *Reliability Engineering & System Safety* **191**, 106550 (2019).
  - [4] A. D. Jenkins, M. B. Paskyabi, I. Fer, A. Gupta, and M. Adakudlu, Modelling the effect of ocean waves on the atmospheric and ocean boundary layers, *Energy Procedia* **24**, 166 (2012).
  - [5] O. Ferčák, J. Bossuyt, N. Ali, and R. B. Cal, Decoupling wind–wave–wake interactions in a fixed-bottom offshore wind turbine, *Applied Energy* **309**, 118358 (2022).
  - [6] P. McKay, R. Carriveau, D. S. Ting, and T. Newson, Turbine wake dynamics, in *Advances in Wind Power* (IntechOpen, 2012).
  - [7] G. Marmidis, S. Lazarou, and E. Pyrgioti, Optimal placement of wind turbines in a wind park using monte carlo simulation, *Renewable energy* **33**, 1455 (2008).
  - [8] K. E. Johnson and N. Thomas, Wind farm control: Addressing the aerodynamic interaction among wind turbines, in 2009 American Control Conference (IEEE, 2009) pp. 2104–2109.
  - [9] Y. Wang, W. Miao, Q. Ding, C. Li, and B. Xiang, Numerical investigations on control strategies of wake deviation for large wind turbines in an offshore wind farm, *Ocean Engineering* **173**, 794 (2019).
  - [10] W. Tian, A. Ozbay, and H. Hu, An experimental investigation on the wake interferences among wind turbines sited in aligned and staggered wind farms, *Wind Energy* **21**, 100 (2018).
  - [11] W. Yue, C. Meneveau, M. B. Parlange, W. Zhu, R. Van Hout, and J. Katz, A comparative quadrant analysis of turbulence in a plant canopy, *Water resources research* **43** (2007).
  - [12] N. Hamilton, H. Suk Kang, C. Meneveau, and R. Bayoán Cal, Statistical analysis of kinetic energy entrainment in a model wind turbine array boundary layer, *Journal of renewable and sustainable energy* **4**, 063105 (2012).
  - [13] K. P. Nolan and T. A. Zaki, Conditional sampling of transitional boundary layers in pressure gradients, *Journal of Fluid Mechanics* **728**, 306 (2013).
  - [14] M. P. Buckley and F. Veron, The turbulent airflow over wind generated surface waves, *European Journal of Mechanics-B/Fluids* **73**, 132 (2019).
  - [15] R. Antonia and L. Browne, Quadrant analysis in the turbulent far-wake of a cylinder, *Fluid dynamics research* **2**, 3 (1987).
  - [16] G. Fabris, Conditional sampling study of the turbulent wake of a cylinder. part 1, *Journal of Fluid Mechanics* **94**, 673 (1979).
  - [17] W. Zhu, R. Van Hout, L. Luznik, H. Kang, J. Katz, and C. Meneveau, A comparison of piv measurements of canopy turbulence performed in the field and in a wind tunnel model, *Experiments in fluids* **41**, 309 (2006).
  - [18] K. Viestenz and R. B. Cal, Streamwise evolution of statistical events in a model wind-turbine array, *Boundary-layer meteorology* **158**, 209 (2016).
  - [19] R. B. Cal, J. Lebrón, L. Castillo, H. S. Kang, and C. Meneveau, Experimental study of the horizontally averaged flow structure in a model wind-turbine array boundary layer, *Journal of renewable and sustainable energy* **2**, 013106 (2010).
  - [20] S. Shamsoddin and F. Porté-Agel, Large-eddy simulation of atmospheric boundary-layer flow through a wind farm sited on topography, *Boundary-layer meteorology* **163**, 1 (2017).
  - [21] C. S. Ferreira, G. Van Kuik, G. Van Bussel, and F. Scarano, Visualization by piv of dynamic stall on a vertical axis wind turbine, *Experiments in fluids* **46**, 97 (2009).
  - [22] I. Naumov, R. F. Mikkelsen, V. Okulov, and J. N. Sørensen, Piv and lda measurements of the wake behind a wind turbine model, in *Journal of Physics: Conference Series*, Vol. 524 (IOP Publishing, 2014) p. 012168.
  - [23] Z. Jin, Q. Dong, and Z. Yang, A stereoscopic piv study of the effect of rime ice on the vortex structures in the wake of a wind turbine, *Journal of Wind Engineering and Industrial Aerodynamics* **134**, 139 (2014).
  - [24] M. P. Buckley and F. Veron, Airflow measurements at a wavy air–water interface using piv and lif, *Experiments in Fluids*

- 58**, 1 (2017).
- [25] D. Yang, C. Meneveau, and L. Shen, Dynamic modelling of sea-surface roughness for large-eddy simulation of wind over ocean wavefield, *Journal of Fluid Mechanics* **726**, 62 (2013).
  - [26] S. Xiao and D. Yang, Large-eddy simulation-based study of effect of swell-induced pitch motion on wake-flow statistics and power extraction of offshore wind turbines, *Energies* **12**, 1246 (2019).
  - [27] Y. Odemark and J. H. Fransson, The stability and development of tip and root vortices behind a model wind turbine, *Experiments in fluids* **54**, 1 (2013).
  - [28] Z. Yang, P. Sarkar, and H. Hu, Visualization of the tip vortices in a wind turbine wake, *Journal of visualization* **15**, 39 (2012).
  - [29] P. McKay, R. Carriveau, and D. S. Ting, Farm wide dynamics: the next critical wind energy frontier, *Wind Engineering* **35**, 397 (2011).
  - [30] J. F. Manwell, J. G. McGowan, and A. L. Rogers, Wind energy explained: theory, design and application (John Wiley & Sons, 2010).
  - [31] T. Burton and D. Sharpe, N. Jenkins, and e. Bossanyi, *Wind Energy Handbook*, 61 (2001).
  - [32] K. Thomsen and P. Sørensen, Fatigue loads for wind turbines operating in wakes, *Journal of Wind Engineering and Industrial Aerodynamics* **80**, 121 (1999).
  - [33] S. J. Andersen, J. N. Sørensen, and R. F. Mikkelsen, Turbulence and entrainment length scales in large wind farms, *Philosophical Transactions of the Royal Society A: Mathematical, Physical and Engineering Sciences* **375**, 20160107 (2017).
  - [34] M. Raupach, Conditional statistics of Reynolds stress in rough-wall and smooth-wall turbulent boundary layers, *Journal of Fluid Mechanics* **108**, 363 (1981).
  - [35] D. Poggi, G. Katul, and J. Albertson, Momentum transfer and turbulent kinetic energy budgets within a dense model canopy, *Boundary-Layer Meteorology* **111**, 589 (2004).